Molecular Vision 2016; 22:332-341 <http://www.molvis.org/molvis/v22/332>
Received 15 December 2015 | Accepted 8 April 2016 | Published 11 April 2016

Myelin-specific Th17 cells induce severe relapsing optic neuritis with irreversible loss of retinal ganglion cells in C57BL/6 mice

Chelsea M. Larabee,[1,2] Yang Hu,[3] Shruti Desai,[2] Constantin Georgescu,[3] Jonathan D. Wren,[3] Robert C. Axtell,[3] Scott M. Plafker[1,2]

[1]Oklahoma Center for Neuroscience, University of Oklahoma Health Sciences Center, Oklahoma City, OK; [2]Aging and Metabolism Research Program, Oklahoma Medical Research Foundation, Oklahoma City, OK; [3]Arthritis and Clinical Immunology Research Program, Oklahoma Medical Research Foundation, Oklahoma City, OK

Purpose: Optic neuritis affects most patients with multiple sclerosis (MS), and current treatments are unreliable. The purpose of this study was to characterize the contribution of Th1 and Th17 cells to the development of optic neuritis.
Methods: Mice were passively transferred myelin-specific Th1 or Th17 cells to induce experimental autoimmune encephalomyelitis (EAE), a model of neuroautoimmunity. Visual acuity was assessed daily with optokinetic tracking, and 1, 2, and 3 weeks post-induction, optic nerves and retinas were harvested for immunohistochemical analyses.
Results: Passive transfer experimental autoimmune encephalomyelitis elicits acute episodes of asymmetric visual deficits and is exacerbated in Th17-EAE relative to Th1-EAE. The Th17-EAE optic nerves contained more inflammatory infiltrates and an increased neutrophil to macrophage ratio. Significant geographic degeneration of the retinal ganglion cells accompanied Th17-EAE but not Th1.
Conclusions: Th17-induced transfer EAE recapitulates pathologies observed in MS-associated optic neuritis, namely, monocular episodes of vision loss, optic nerve inflammation, and geographic retinal ganglion cell (RGC) degeneration.

Optic neuritis (ON), optic nerve inflammation, is the presenting clinical symptom for 19% of patients with multiple sclerosis (MS) and occurs in more than 50% of patients during disease progression [1]. ON is characterized by acute reductions of central visual acuity, color vision, visual field size, and afferent pupillary function [2]. Recovery usually begins 2 weeks after onset and is typically complete within 6 months [3]. ON causes demyelination of the optic nerve, thinning of the retinal nerve fiber layer (RNFL), and death of retinal ganglion cells (RGCs), all of which can contribute to incomplete vision recovery [4]. Standard steroid treatment accelerates recovery for only 30% of patients and does not affect long-term recovery or relapse frequency [5].

Active experimental autoimmune encephalomyelitis (EAE) is a well-established MS model induced by immunization of mice against myelin antigen; EAE recapitulates the cardinal hallmarks of ON [6]. Previous work demonstrated that Th17 cells are necessary for EAE induction [7-9]. Although interleukin (IL)-17 and interferon gamma (IFN-γ) are upregulated in temporally distinct patterns in the optic nerves of active EAE mice [10], the roles of these two T-cell pathways in visual deficits, optic nerve inflammation, and RGC degeneration have not been explored.

Correspondence to: Scott M Plafker, Aging and Metabolism Research Program, Oklahoma Medical Research Foundation, 825 NE 13th St, OKC, OK 73104; Phone : (405) 271-1735; FAX: (405) 271-1437; email: PlafkerS@omrf.org

In patients with MS [11] and active mouse EAE [12], visual evoked potential (VEP) recovery after episodes of ON do not always correlate to changes in visual acuity. We therefore used a functional assay that takes advantage of the optokinetic reflex (OKT). Similar to nystagmus in humans, this reflex stabilizes a moving image on the retina, resulting in the mouse head moving with the stimulus [12]. The OKT threshold is a non-invasive assessment of visual function that tests only one eye at a time (as the reflex is selectively temporal to nasal) and does not induce fatigue or adaption with repeated testing [13].

In this study, we characterized the visual deficits and corresponding optic nerve inflammation and RGC loss in two passive transfer EAE models induced by myelin-specific Th1 or Th17 cells. Both models exhibited episodic, asymmetric visual deficits that were exacerbated in Th17-EAE. General inflammation and the ratio of neutrophils to macrophages were increased in Th17-EAE relative to Th1. Only Th17-EAE mice exhibited significant loss of central retina RGCs.

METHODS

Mice: All animal care was performed in compliance with the guidelines of the OMRF Institutional Animal Care and Use Committee and the study was adhered to ARVO Statement for Use of Animals in Research. Eight-week-old female C57BL/6 mice purchased from the Jackson Laboratory (Bar Harbor, ME) were housed in an Assessment and Accreditation

of Laboratory Animal Care–approved vivarium, given ad libitum access to chow and water, and exposed to a standard 14 h:10 h light-dark cycle.

Passive transfer EAE: Eight- to twelve-week-old donor mice were immunized subcutaneously with 150 µg $MOG_{35–55}$ (Bio-Synthesis Inc., Lewisville, TX) emulsified in complete Freund's adjuvant (CFA; Difco Laboratories Inc., Franklin Lakes, NJ) containing 2.5 mg/ml heat-killed *Myobacterium tuberculosis*. Mice were injected intraperitoneally with 250 ng *Bordetella pertussis* toxin (Difco Labs) the day of, and 2 days following, $MOG_{35–55}$ immunization. Ten days post-immunization (DPI), spleen and draining lymph nodes were mechanically disrupted to obtain cell suspensions. Cells were restimulated with 10 µg/ml $MOG_{35–55}$ with 10 ng/ml IL-12 (Th1) or IL-23 (Th17; R&D Systems Inc., Minneapolis, MN) for 3 days before i.p. injection of $1×10^7$ cells into healthy 9-week-old recipients. Thirty recipient mice (15 Th1 and 15 Th17) were used, with five from each group harvested at 8, 13, and 21 DPI for histological analyses. EAE clinical manifestations of progressive ascending paralysis were assessed daily using a standard scoring system: 1 = loss of tail tone, 2 = hind limb paresis, 3 = complete hind limb paralysis, 4 = hind limb paralysis and forelimb paresis, 5 = moribund or dead. Mice were weighed daily to ensure weight loss did not exceed 25% of starting weight.

Visual acuity assessment: Visual acuity threshold was measured daily by OKT response using Optometry software and apparatus (Cerebral Mechanics Inc., Alberta, Canada) as previously described [14]. Mice were placed on a raised platform surrounded by a virtual cylinder consisting of vertical lines at 100% contrast rotating at varying frequencies. Mice were observed through a camera, and tracking behavior was assessed by an investigator blinded to the treatments. Visual acuity is represented as the highest spatial frequency at which mice track the rotating cylinder. Because tracking is a temporal to the nasal-specific reflex, counter-clockwise and clockwise rotation exclusively test right and left eye, respectively.

Optic nerve H&E analysis: Mice were euthanized by CO_2 asphyxiation and perfused with PBS (1X; 137 mM NaCl, 27 mM KCl, 10 mM Na_2HPO_4, 2 mM KH_2PO_4, pH 7.5), and the optic nerves were fixed in 10% neutral buffered formalin (NBF) for 2–5 h before paraffin-embedding in a Shandon Excelsior tissue processor (Thermo Fisher Scientific, Waltham, MA) as described [15]. Longitudinal, 5 µm sections were cut using a Leica Instruments microtome (model 2045 Multicut; Leica, Wetzlar, Germany) and mounted on charged glass slides. Two slides per optic nerve corresponding to the lateral and medial longitudinal plane were hematoxylin and eosin (H&E) stained, and inflammation scores were averaged from both sections. Slides were deparaffinized with serial washes in xylene, ethanol, and distilled water before 5 min incubation in Gill's hematoxylin. Water was run over the slides for 5 min before 30 s incubation in Eosin Y with phloxine. After a tap water rinse, the slides were dehydrated by serial incubation in increasing ethanol and then xylene before being coverslipped with Permount mounting medium (Thermo Fisher Scientific). Slides were viewed on a Nikon (Tokyo, Japan) Eclipse E200 and imaged with a Nikon DS-Fi1 camera with NIS Elements software, and 10X images were merged in Adobe Photoshop 8.0 (San Jose, CA). Optic nerve pictures were graded for inflammation by a blinded investigator according to the following scale: 0 = absent or minimal infiltrates, 1 = moderate infiltrates throughout, 2 = moderate infiltrates with severe areas, 3 = severe infiltrates throughout.

Optic nerve immunohistochemistry: Two slides per nerve (neighboring H&E-analyzed slides) were deparaffinized by serial washes in Histo-clear (National Diagnostics, Atlanta, GA), ethanol, and distilled water before heat-induced epitope retrieval using a Retriever 2100 (Electron Microscopy Sciences, Hatfield, PA) in the accompanying R-buffer B. Slides cooled in the retriever for 4–20 h before incubation in blocking solution (10% goat serum + 3% bovine serum albumin (BSA) in PBS) for 1–3 h at room temperature (RT). Sections were incubated at 4 °C overnight in blocking solution containing primary antibody. Primary antibodies used were anti-B220 (B-cells; BioLegend, San Diego, CA, cat# 103201; 1:400), anti-CD3 (T-cells; Abcam, Cambridge, MA, cat# ab5690; 1:250), anti-Iba1 (macrophages and microglia; Millipore, Darmstadt, Germany, cat# MABN92; 1:50), anti-CNPase (myelin; Covance, Princeton, NJ, cat# SMI-91R; 1:500), and anti-Ly6G (neutrophils; Abcam, cat# ab25377; 1:250). Slides were washed in PBS and incubated in secondary antibody ($Alexa_{488/546/647nm}$ Fluor-conjugated goat anti-rat/mouse/rabbit immunoglobulin G (IgG; Molecular Probes, Eugene, OR) at 1:500) and Hoechst 33342 (2 µg/ml) in 3% BSA/PBS for 1 h at RT. After a final PBS wash, the slides were mounted using ProLong Gold (Cell Signaling Technology, Boston, MA) and examined with a Nikon 80i microscope and DXM1200C camera. Separate gray-scale images for each channel were captured using NIS-Elements software (Nikon), and representative images were processed in Adobe Photoshop (Version 8.0). Analysis was performed on raw images using NIH ImageJ software. B220- or CD4-positive cells were counted in three representative fields throughout each nerve and are represented as number of cells. Iba1- and CNPase-positive cells are represented as average percent area stained in three representative fields due to diffuse staining. Ly6G staining was quantitated using a

binning method with a score of 0 indicating no Ly6G signal, 1 indicating 1–15 Ly6G-positive cells throughout the section, 2 indicating 16–30 Ly6G-positive cells, and 3 indicating greater than 30 Ly6G-positive cells.

Retinal flatmount analysis: Eyes were enucleated in 10% NBF and fixed for 3 h. Under a dissecting microscope (Olympus SZ-PT, Center Valley, PA), the corneas were punctured for fixation with the lens intact for an additional 30–60 min. Retinas were isolated and permeabilized in 1% Triton X-100/PBS for 30 min before incubation in blocking solution (10% donkey serum + 3% BSA in PBS) for 1–3 h. Retinas were incubated at 4 °C overnight in the RGC-specific antibody anti-Brn3a (Santa Cruz, Santa Cruz, CA; sc31984; 1:500) in blocking solution followed by PBS washes and incubation with $Alexa_{488nm}$ Fluor-conjugated donkey anti-goat IgG (1:1,000; Molecular Probes) and Hoechst 33342 (2 µg/ml) in 3% BSA/PBS for 1 h, and additional PBS washes and then were cut to lie flatly before mounting with Prolong Gold mounting medium (Life Technologies, Grand Island, NY). Retinas were viewed with an LSM-710 confocal (Carl Zeiss, Jena, Germany) using widefield settings and imaged with Zeiss Axiocam HRM camera using Axioobserver Z1 running Zen Black 2012 capable of tiled imaging and stitching to produce high-resolution images of whole retinas. The central retina is more populated with RGCs than the peripheral retina, and flatmounts consist of four quadrants; therefore, representative fields (325 μm^2) from the peripheral, medial, and central retina within each quadrant were analyzed, totaling 12 pictures per retina. Images were processed identically in Adobe Photoshop 8.0. Using NIH ImageJ software, images were subjected to a user-defined threshold such that only Brn3a-positive areas were represented, and the "Analyze particles" function was used to count individual regions of interest (RGCs).

Data collection design: At 0 DPI, 15 naïve recipient mice were injected with myelin-specific Th1 cells and 15 other mice with myelin-specific Th17 cells. Longitudinal EAE motor scores and OKTs were collected daily until the day of harvest, at which time the optic nerves and eyes were collected. At 8, 13, and 21 DPI, five mice of each group were harvested such that the biologic replicates for 0–8, 9–12, and 13–21 DPI were 15, 10, and 5, respectively. For the optic nerve analyses (H&E and immunohistochemical), two slides corresponding to the medial and lateral planes were assessed to give one final value per nerve. For immunohistochemical quantitation, three representative fields were averaged to represent that section of the optic nerve. The values for central, medial, and peripheral RGCs in the retinas are the sum of four representative fields from each of the four quadrants within each flatmount. In the analyses that included both eyes (as opposed to only more or less affected), sound statistical handling of the correlated values was achieved by proper specification of the random effect structure in the estimating linear mixed models used in the data analysis process.

Statistical analysis: Confidence intervals and p values for the significance of each studied effect were mostly determined by fitting the data to a linear mixed effects model, using the lme function implemented in the nlme R package. This function is an extended version of regular linear regression but can accommodate complex data collection design features such as longitudinal measurements, nested layers, and within-group correlation. The method formulation [16], computational method [17], and implementation of the model in R [18] have previously been described. Proper handling of the multilayer embedded data collection design was achieved by correct specification of the random effect structure in the corresponding parameter of the lme function (mouse/eye for longitudinal OKT and EAE data and mouse/eye/eye region for RGC analyses). Fixed-effect coefficient tables were extracted with the table method while confidence intervals were returned by the intervals function in the nlme package. When suitable (optic nerve immunohistochemistry), log-transformed versions of the variables toward normality were used in the analysis to better fulfill the functions of the statistical procedures. Standard testing methods, such as ANOVA, the *t* test, or Mann–Whitney's exact test, were employed when no embedding was involved. One-sided or two-sided testing was chosen individually, for each effect, according to the predictability of the outcome.

RESULTS

This study was undertaken to fully characterize the ocular pathology in two variations of MOG-specific passive transfer EAE. This work is distinguished from previous studies by assessing whether visual deficits are (1) episodic, constant, or progressive over time, (2) monocular or binocular, (3) correlated with optic nerve inflammation and loss of RGCs, and (4) more attributable to the Th1 or Th17 arm of the autoimmune response.

Th1- and Th17-EAE induce acute episodes of asymmetric visual impairment: Th1- or Th17-EAE was induced in 15 mice each, and visual acuity and paralysis were assessed daily. At 8, 13, and 21 DPI, five mice from each group were harvested for histological analyses (Figure 1). Th1 and Th17 transfer EAE, elicited acute, asymmetric decreases in visual acuity that coincided with the initial onset of motor symptoms and resolved within several days (Figure 2A). Subsequent episodes of visual dysfunction commonly occurred in the

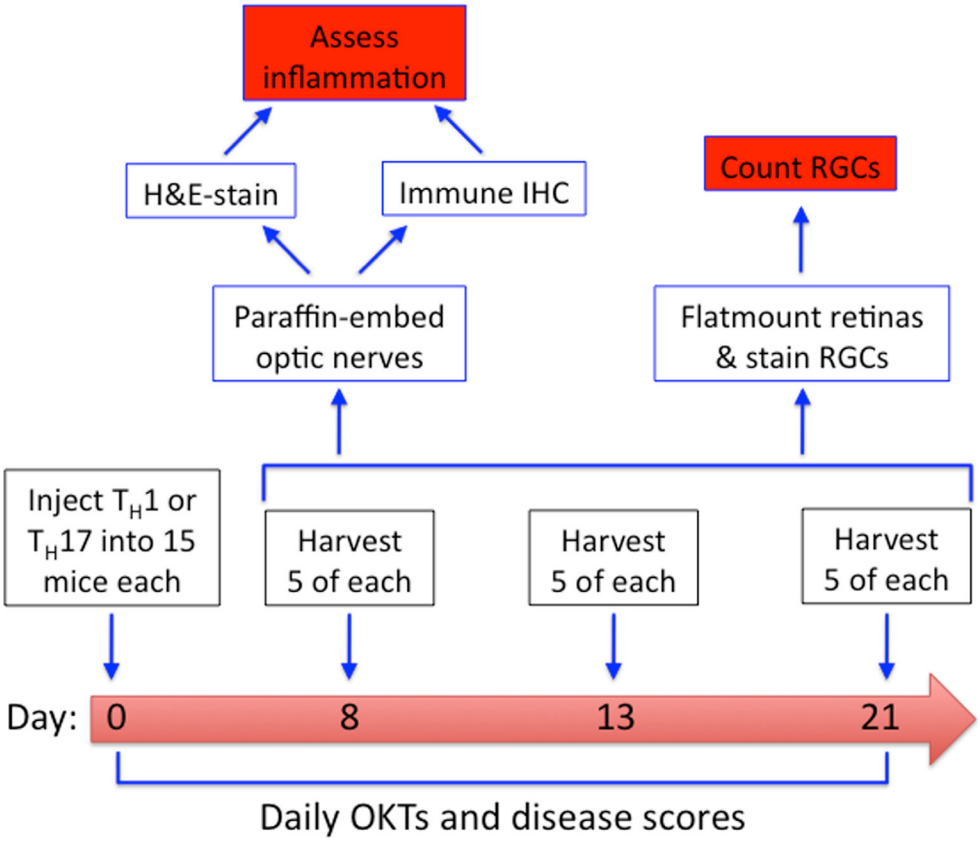

Figure 1. Experimental design. Cultured, myelin-specific Th1 (interleukin (IL)-12-treated) or Th17 (IL-23-treated) cells were injected into 15 naïve recipient mice each, and optokinetic reflexes (OKTs) and disease severity were assessed daily. At approximately 1, 2, and 3 weeks post-induction, five mice from each group were harvested. The optic nerves were histologically assessed for inflammation, and retinal ganglion cells (RGCs) were counted in retinal flatmounts.

same eye (Figure 2A–C). Most mice had an eye that exhibited more severe visual deficits (termed "more affected eye" [MA]) and an eye with much less or no vision loss (termed "less affected eye" [LA]; Figure 2B–F). There was no left or right eye predominance. At all three time points, both groups exhibited significant asymmetric deficits (Figure 2D–F). Previous studies measured the visual acuity of active EAE mice on a weekly basis [6,12,19,20], but by performing daily OKTs, we found that, unlike previous reports, visual deficits occur as acute relapsing episodes, in contrast to the sustained paralysis typical of EAE in C57BL/6 mice.

Th17-EAE mice exhibit more severe paralysis and visual deficits relative to Th1 mice: Representing the same OKT data from Figure 2 in a different format revealed that Th17-EAE induced more severe deficits in visual acuity than Th1-EAE (Figure 3B–C), although both models exhibited the same kinetics of motor disease onset (Figure 3A). Most mice experienced decreased visual acuity in only one eye, but a small portion (one of ten) of the Th17-EAE mice exhibited binocular deficits, as shown by the lowest point for the Th17 LA eye area under the curve (AUC; Figure 2E–F). The vision of Th1-EAE, but not Th17-EAE, mice fully recovered after the first episode of visual decrease (Figure 3B).

Th17-EAE induces more severe optic nerve infiltration relative to Th1-EAE: We next determined whether decreased visual acuity correlated with optic neuritis. The H&E-stained optic nerve sections were blindly graded for inflammation using a severity scale of 0 to 3 (Figure 4A). Overall, we observed a negative correlation between visual acuity and optic nerve infiltration such that nerves with increased inflammatory infiltrates corresponded to eyes that exhibited lower visual acuity (Figure 4B). Due to the limited binning analysis, the difference in nerve inflammation was statistically significant ($p = 0.0281$) only at 21 DPI (Figure 4C).

Th17-EAE mice exhibit a higher ratio of neutrophils to macrophages relative to Th1-EAE: To determine the cell types driving optic nerve inflammation, sections were stained with cell type-specific antibodies. As there were no significant differences in any parameters at 8 DPI, we focused on 13 and 21 DPI. No statistically significant differences were observed in demyelination (Figure 5A), T-cells (Figure 5B), B-cells (Figure 5C), macrophages/microglia (Figure 5D), or neutrophils (Figure 5E). Th17-EAE mice did, however, have a significantly higher ratio of neutrophils to macrophages and microglia (Figure 5F, $p = 0.0050$).

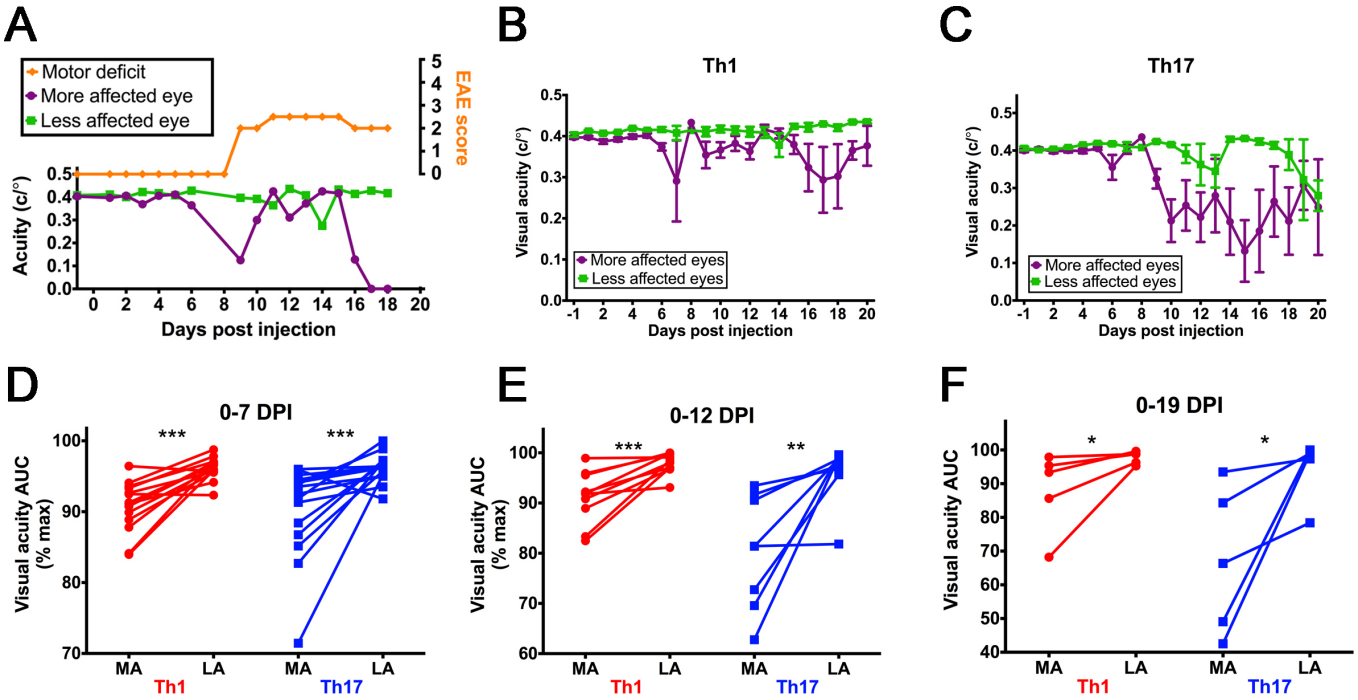

Figure 2. EAE visual deficits are asymmetric and episodic. **A**: Representative time course of optokinetic reflex (OKT) measurements (purple circles and green squares) and disease severity scores (top, orange diamonds) for a transfer experimental autoimmune encephalomyelitis (EAE) mouse demonstrating the asymmetric and episodic nature of visual deficits, the onset of which coincide with motor deficits. **B**, **C**: Means of daily acuity readings (cycles per degree) as measured by OKT for the more affected eyes (purple circles) and less affected eyes (green squares) of the Th1 (**B**) and Th17 (**C**) transfer EAE mice. Error bars represent standard error of the mean (SEM). Number of eyes: n = 15 for 1–7 days post-immunization (DPI), n = 10 for 8–12 DPI, and n = 5 for 13–21 DPI. **D**, **E**, **F**: Area under the curve (AUC; presented as % of maximum for each plot) for daily visual acuity values (cycles per degree) as measured by OKT for each Th1 (left, red circles) and Th17 (right, blue squares) mouse for 0–7 DPI (n = 15; **D**), 0–12 DPI (n = 10; **E**), and 0–19 DPI (n = 5; **F**). Eyes from the same mouse are connected by a line. MA = more affected eye and LA = less affected eye for each mouse as determined by the average OKT score for each eye. *p<0.05, **p<0.01, ***p<0.001 with one-tailed Wilcoxon matched-pairs test.

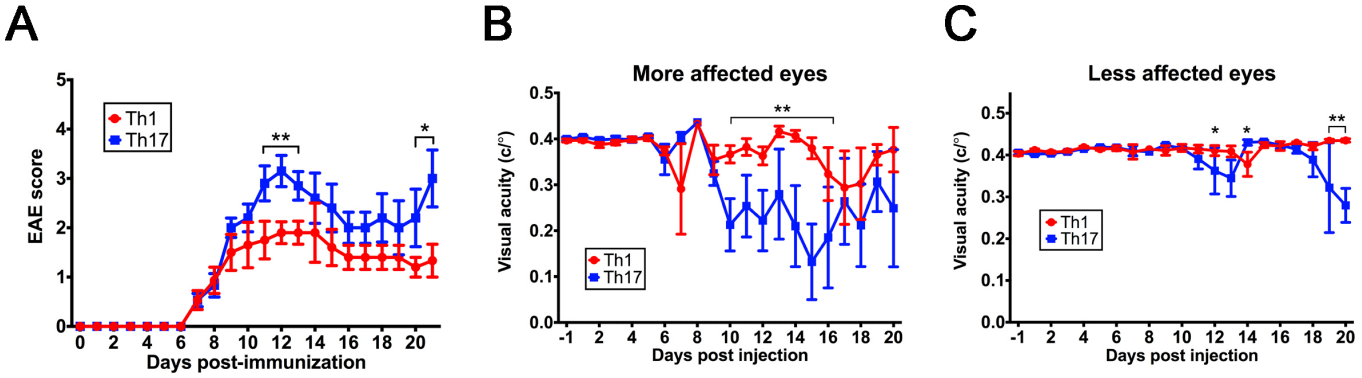

Figure 3. The Th17 transfer EAE model exhibits more severe motor and vision deficits relative to Th1. **A**: Daily mean experimental autoimmune encephalomyelitis (EAE) severity scores for Th1 (red circles) and Th17 (blue squares) transfer EAE mice. **B, C**: Daily mean acuity of more (**B**) or less (**C**) affected eyes of Th1 (red circles) and Th17 (blue squares) mice as measured by optokinetic reflex (OKT) where the more affected eye of each mouse is classified as that with the lower average OKT value over the course of the study. Error bars represent standard error of the mean (SEM). Number of eyes: n = 15 for −1–7 days post-immunization (DPI), n = 10 for 8–12 DPI, and n = 5 for 13–21 DPI. *p<0.05; **p<0.005 with the linear mixed effect model.

Th17-EAE mice exhibit more RGC cell death relative to Th1-EAE: To determine whether loss of RGCs accompanies visual acuity deficits, the retinas isolated at 13 and 21 DPI were flatmounted and immunolabeled for RGCs. RGCs were quantified in 12 representative fields using four images each from peripheral, medial, and central areas of the retina (Figure 6A). We observed a correlation between average acuity and total RGC abundance such that eyes with fewer RGCs exhibited more severe visual acuity deficits (Figure 6B). Significant RGC loss was observed only in mice with Th17-EAE (Figure 6C,D) and, surprisingly, was not global, but geographic in nature, with loss detected in the central retina at 13 and 21 DPI (Figure 6C). Cell loss was most pronounced in the more affected eyes at 21 DPI and radiated from the central to the medial retina (Figure 6D) whereas the peripheral retina was spared. This pattern of RGC dropout around the optic nerve head is similar to MS ON [4].

DISCUSSION

This work represents the first in-depth study of functional visual impairments in Th1- and Th17-EAE and correlates these deficits with inflammation and neurodegeneration of the optic nerve. Daily OKT analyses revealed the novel observation that the induced visual deficits are asymmetric and episodic, contrasting with the chronic paralysis characteristic of EAE in C57BL/6 mice. Therefore, although motor deficits are more progressive in nature with moderate recovery after peak disease, vision loss is more relapsing-remitting in nature. The mechanisms behind these differences in motor and visual disease patterns remain to be fully elaborated.

Our finding that Th17-EAE elicits more severe ocular disease relative to Th1-EAE is consistent with previous studies that assessed brain and spinal cord pathology [21]. The characteristics of Th1- and Th17-induced visual pathology are reminiscent of relapsing-remitting MS (RRMS)

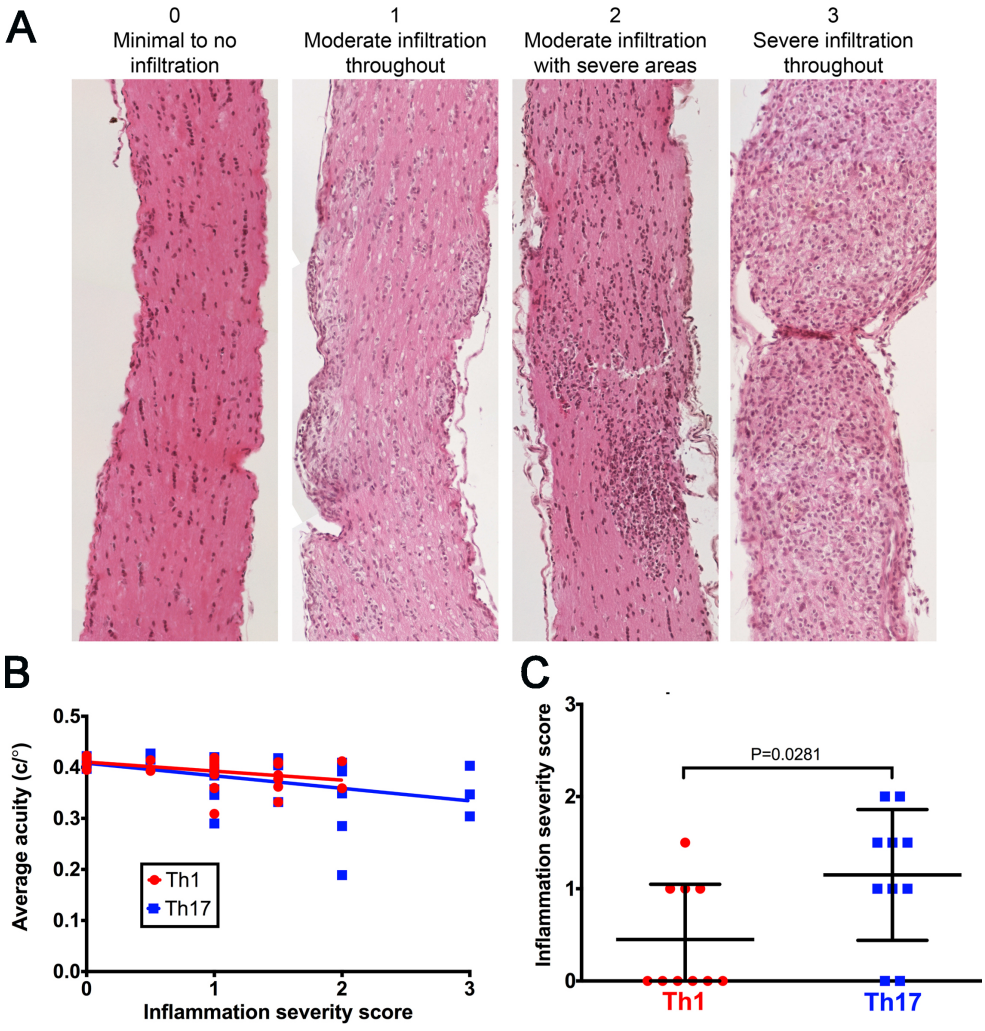

Figure 4. Optic nerve inflammation negatively correlates with visual acuity and is more severe in Th17-EAE relative to Th1. **A**: Representative hematoxylin and eosin (H&E)-stained paraffin-embedded 5-µm optic nerve sections indicating criterion by which all nerves were graded for inflammation severity on a scale of 0–3. **B**: Linear regression of average optokinetic reflex (OKT) values on optic nerve inflammation severity scores throughout the study for the corresponding eye for Th1 (red circles, p = 0.0139) and Th17 (blue squares, p = 0.0055) at 8, 13, and 21 days post-immunization (DPI) indicating significant negative correlations by Spearman correlation. n = 30 eyes (from 15 mice) per group. **C**: Optic nerve inflammation severity scores for Th1 (red circles) and Th17 (blue squares) optic nerves indicating significantly more inflammation in Th17 nerves harvested at only 21 DPI (n = 10 eyes from five mice, p = 0.0281) with an unpaired *t* test.

and neuromyelitis optic (NMO), respectively. RRMS tends to exhibit nearly full recovery after initial visual episodes whereas NMO is an opticospinal demyelinating disease characterized by incomplete recovery with severe RGC loss and higher incidence of bilateral deficits [22]. Most patients with NMO produce autoantibodies against aquaporin 4 (AQP4), a water channel highly concentrated in astrocytes of the optic nerve, but approximately 25% of patients with NMO are AQP4-seronegative and positive for MOG-specific autoantibodies [23]. Moreover, it has been reported that patients with NMO have elevated levels of Th17 cytokines in their serum and spinal fluid compared to patients with RRMS [24,25]. Our results indicate that Th17-EAE may be an appropriate model for AQP4-seronegative NMO.

As the H&E results show significantly more infiltrating cells in the Th17 nerves relative to Th1, there is likely a slight difference in many (or all) cell types instead of a large difference in one type. We found a highly significant increase in the neutrophil to macrophage ratio between the disease models (p = 0.0050, Figure 5F), consistent with the known mechanisms of the Th17 system. Th17 cells release IL-17, which in multiple models of inflammation has been shown to induce the expression of IL-8, granulocyte colony-stimulating factor, and Gro-alpha and culminate in the recruitment of neutrophils [24,26-28]. Previous work demonstrated that spinal cord neutrophil infiltration coincides with motor disease onset and peak [29] and that inhibition of neutrophil migration suppresses EAE onset [30]. Moreover, in a mammalian central nervous system (CNS) bacterial infection model, it was shown that neutrophils can invade the axonal space underneath intact myelin sheath [31]. Taken together, these observations may explain why, although the extent of demyelination and the abundance of other immune cell types are not different between Th1- and Th17-EAE optic nerves, the neutrophil to macrophage composition could primarily be responsible for the increased visual deficits and RGC dropout in Th17-EAE.

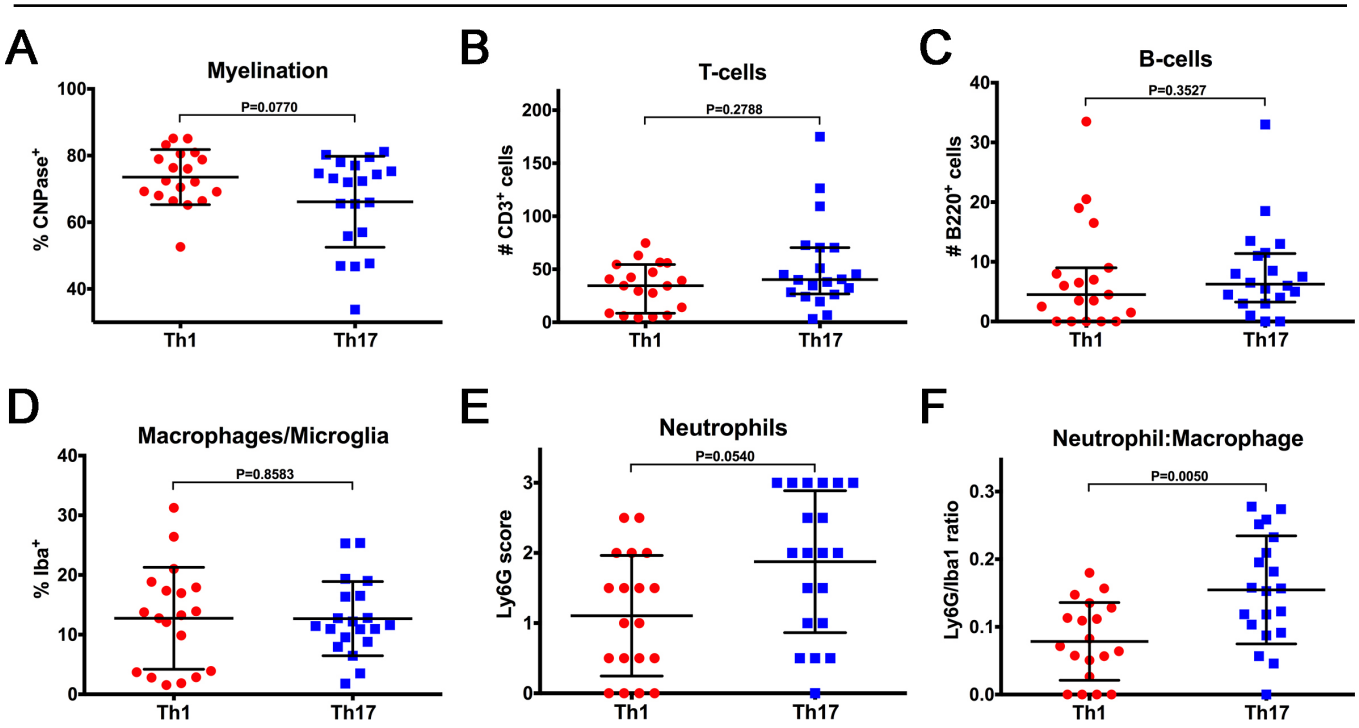

Figure 5. Th17-induced optic neuritis consists of a higher neutrophil to macrophage ratio relative to Th1. Quantitation of cell type-specific markers in paraffin-embedded optic nerves from mice harvested at 13 and 21 days post-immunization (DPI). Each nerve is represented as the average value from two separate longitudinal sections. **A**: Myelination as measured by the percentage of nerves positive for the anti-CNPase signal, p = 0.0770. **B**: T-cells as measured by the number of CD3-positive cells counted in three representative 20X fields throughout each section, p = 0.2788. **C**: B-cells as measured by the number of B220-positive cells counted in three representative 20X fields throughout each section, p = 0.3527. **D**: Macrophage and microglia infiltration as measured by the percentage of nerves positive for the anti-Iba1 signal, p = 0.8583. **E**: Neutrophil infiltration scored on a scale of 0–3 for the anti-Ly6G signal where 0 = no signal, 1 = 1–15 cells, 2 = 16–30 cells, and 3 = more than 30 cells, p = 0.0540. **F**: The ratio of the Ly6G:Iba1 values for each optic nerve, p = 0.0050. All comparisons made with a linear mixed effect model. Testing for B220, CD3, and CNPase effects was performed on a log scale. Error bars represent standard deviation (SD). n = 20 eyes from ten mice per group.

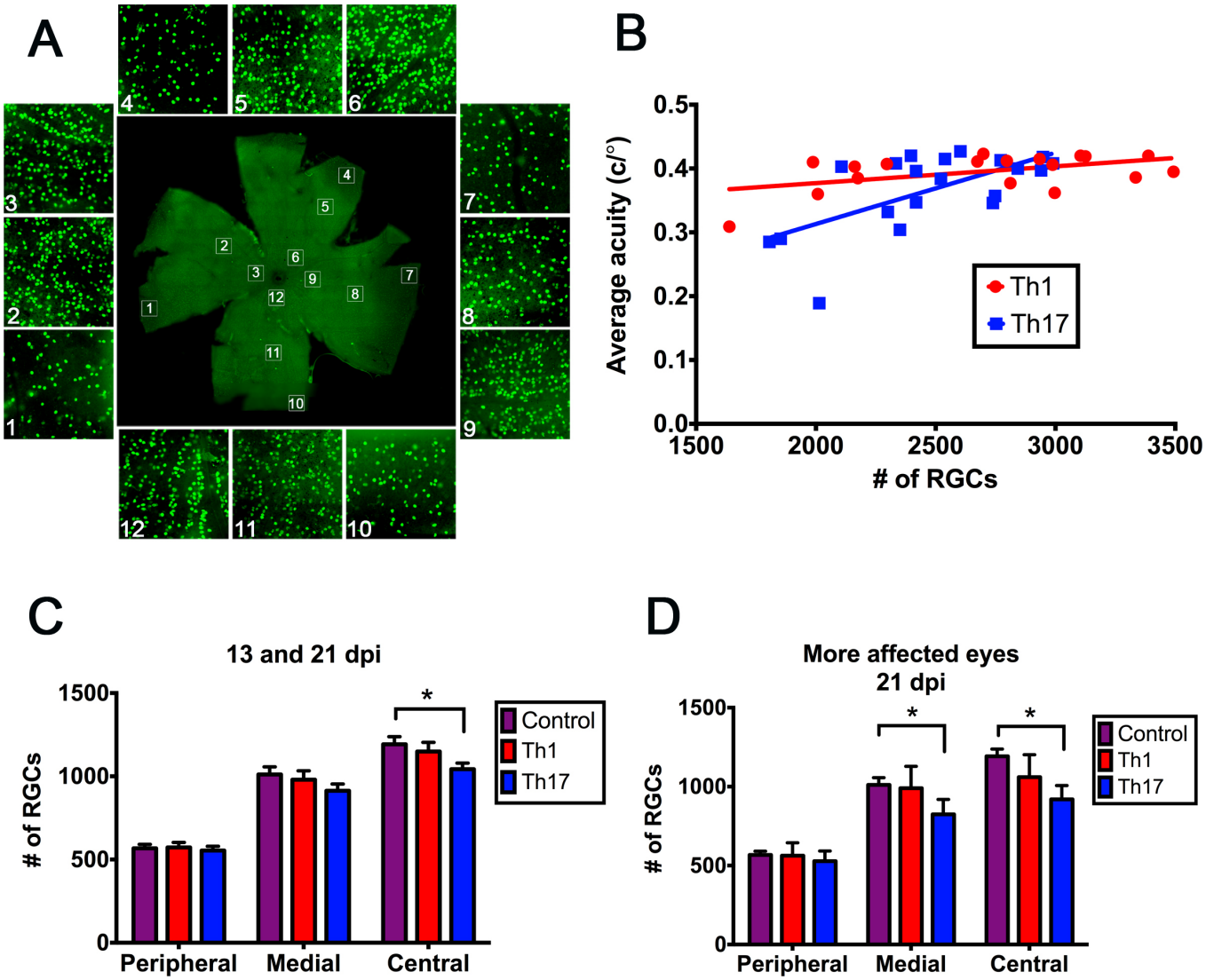

Figure 6. Number of RGCs correlates with visual acuity, and RGC death occurs in Th17- but not Th1-induced EAE. **A**: Representative photomicrograph of a retinal flatmount immunostained with anti-Brn3a. White boxes (labeled 1–12) indicate representative fields taken from peripheral (1, 4, 7, 10), medial (2, 5, 8, 11), and central (3, 6, 9, 12) regions of each quadrant. Automated retinal ganglion cell (RGC) counts in the enhanced fields (shown in surrounding pictures) were performed in Image J. **B**: Linear regression of the average optokinetic reflex (OKT) on the total number of RGCs counted in the 12 representative retinal fields throughout the study for each Th1 (red circles, p = 0.0396) and Th17 (blue squares, p = 0.0023) experimental autoimmune encephalomyelitis (EAE) eye at 13 and 21 days post-immunization (DPI) indicating significant positive correlations. n = 20 eyes from ten mice per group. **C**: Average total RGCs counted in each retinal region of all eyes at 13 and 21 dpi for Th1 (red middle bars), Th17 (blue right bars), and healthy, age- and strain-matched control mice (purple left bars). n = 20 eyes from ten mice per group. **D**: Average total regional RGCs counted in the more affected eyes of each EAE mouse at 21 dpi for Th1 (red middle bars), Th17 (blue right bars), and healthy, age-, and strain-matched control mice (purple left bars). n = 5. Error bars represent standard error of the mean (SEM). *p<0.05 by the linear mixed effect model.

At 21 DPI in Th17-mediated EAE, we observed significant loss of medial and central RGCs, whereas at 13 DPI, only central RGC loss was evident. These data suggest RGC loss initially occurs around the optic nerve head and spreads to the medial retina over time, similar to what occurs in patients with MS [4]. This spread to the medial retina may be due to a diffusible factor(s) released by the dying cells.

In summary, we have performed the first in-depth analysis of visual pathology in the Th1- and Th17-EAE models and have made the novel discovery that deficits in visual acuity are asymmetric and relapsing. EAE-associated optic

neuritis is exacerbated in Th17-EAE relative to Th1-EAE in terms of visual acuity loss, inflammation of the optic nerve, and degeneration of the RGCs. Interestingly, RGC loss recapitulated what is observed in patients with MS, as degeneration is most prevalent around the optic nerve head [4]. Overall, these findings are consistent with the Th17 cell population contributing significantly to the incidence of optic neuritis in patients with MS and NMO.

ACKNOWLEDGMENTS

Scott M. Plafker (pPlafkersS@omrf.org) and Robert C. Axtell (axtellb@omrf.org) are co-corresponding authors on this manuscript. This work was supported by intramural funds to S.M.P and R.C.A., Nathan Shock Center Grant P30AG050911 to J.D.W., and a predoctoral fellowship to C.M.L. from OMRF. A portion of this work was presented by C.M.L. in a poster presentation at the Neurobiology of Brain Disorders Gordon Research Seminar & Conference in Girona, Spain on July 27–29, 2014.

REFERENCES

1. Pinholt M, Frederiksen JL, Andersen PS, Christiansen M. Apo E in multiple sclerosis and optic neuritis: the apo E-epsilon4 allele is associated with progression of multiple sclerosis. Mult Scler 2005; 11:511-5. [PMID: 16193886].
2. Kaur P, Bennett JL. Optic neuritis and the neuro-ophthalmology of multiple sclerosis. Int Rev Neurobiol 2007; 79:633-63. [PMID: 17531862].
3. Beck RW, Cleary PA, Backlund JC. The course of visual recovery after optic neuritis. Experience of the Optic Neuritis Treatment Trial. Ophthalmology 1994; 101:1771-8. [PMID: 7800355].
4. Fjeldstad C, Bemben M, Pardo G. Reduced retinal nerve fiber layer and macular thickness in patients with multiple sclerosis with no history of optic neuritis identified by the use of spectral domain high-definition optical coherence tomography. J Clin Neurosci 2011; 18:1469-72. [PMID: 21917458].
5. Brusaferri F, Candelise L. Steroids for multiple sclerosis and optic neuritis: a meta-analysis of randomized controlled clinical trials. J Neurol 2000; 247:435-42. [PMID: 10929272].
6. Quinn TA, Dutt M, Shindler KS. Optic neuritis and retinal ganglion cell loss in a chronic murine model of multiple sclerosis. Front Neurol 2011; 2:50-[PMID: 21852980].
7. Segal BM, Dwyer BK, Shevach EM. An interleukin (IL)-10/IL-12 immunoregulatory circuit controls susceptibility to autoimmune disease. J Exp Med 1998; 187:537-46. [PMID: 9463404].
8. Gran B, Zhang GX, Yu S, Li J, Chen XH, Ventura ES, Kamoun M, Rostami A. IL-12p35-deficient mice are susceptible to experimental autoimmune encephalomyelitis: evidence for redundancy in the IL-12 system in the induction of central nervous system autoimmune demyelination. J Immunol 2002; 169:7104-10. [PMID: 12471147].
9. Cua DJ, Sherlock J, Chen Y, Murphy CA, Joyce B, Seymour B, Lucian L, To W, Kwan S, Churakova T, Zurawski S, Wiekowski M, Lira SA, Gorman D, Kastelein RA, Sedgwick JD. Interleukin-23 rather than interleukin-12 is the critical cytokine for autoimmune inflammation of the brain. Nature 2003; 421:744-8. [PMID: 12610626].
10. Zhang R, Tian A, Shi X, Yu H, Chen L. Downregulation of IL-17 and IFN-gamma in the optic nerve by beta-elemene in experimental autoimmune encephalomyelitis. Int Immunopharmacol 2010; 10:738-43. [PMID: 20399285].
11. Diem R, Tschirne A, Bahr M. Decreased amplitudes in multiple sclerosis patients with normal visual acuity: a VEP study. J Clin Neurosci 2003; 10:67-70. [PMID: 12464525].
12. Matsunaga Y, Kezuka T, An X, Fujita K, Matsuyama N, Matsuda R, Usui Y, Yamakawa N, Kuroda M, Goto H. Visual functional and histopathological correlation in experimental autoimmune optic neuritis. Invest Ophthalmol Vis Sci 2012; 53:6964-71. [PMID: 22969072].
13. Cahill H, Nathans J. The optokinetic reflex as a tool for quantitative analyses of nervous system function in mice: application to genetic and drug-induced variation. PLoS One 2008; 3:e2055-[PMID: 18446207].
14. Prusky GT, Alam NM, Beekman S, Douglas RM. Rapid quantification of adult and developing mouse spatial vision using a virtual optomotor system. Invest Ophthalmol Vis Sci 2004; 45:4611-6. [PMID: 15557474].
15. Larabee CM, Georgescu C, Wren JD, Plafker SM. Expression profiling of the ubiquitin conjugating enzyme UbcM2 in murine brain reveals modest age-dependent decreases in specific neurons. BMC Neurosci 2015; 16:76-[PMID: 26566974].
16. Laird NM, Ware JH. Random-effects models for longitudinal data. Biometrics 1982; 38:963-74. [PMID: 7168798].
17. Lindstrom ML, Bates DM. Nonlinear mixed effects models for repeated measures data. Biometrics 1990; 46:673-87. [PMID: 2242409].
18. Pinheiro JC, Bates DM. Mixed Effects Models in S and S-Plus. New York: Springer-Verlag; 2000.
19. An X, Kezuka T, Usui Y, Matsunaga Y, Matsuda R, Yamakawa N, Goto H. Suppression of experimental autoimmune optic neuritis by the novel agent fingolimod. J Neuroophthalmol 2013; 33:143-8. [PMID: 23609767].
20. Fonseca-Kelly Z, Nassrallah M, Uribe J, Khan RS, Dine K, Dutt M, Shindler KS. Resveratrol neuroprotection in a chronic mouse model of multiple sclerosis. Front Neurol 2012; 3:84-[PMID: 22654783].
21. Axtell RC, de Jong BA, Boniface K, van der Voort LF, Bhat R, De Sarno P, Naves R, Han M, Zhong F, Castellanos JG, Mair R, Christakos A, Kolkowitz I, Katz L, Killestein J, Polman CH, de Waal Malefyt R, Steinman L, Raman C. T helper type 1 and 17 cells determine efficacy of interferon-beta in

multiple sclerosis and experimental encephalomyelitis. Nat Med 2010; 16:406-12. [PMID: 20348925].

22. Wingerchuk DM, Lennon VA, Pittock SJ, Lucchinetti CF, Weinshenker BG. Revised diagnostic criteria for neuromyelitis optica. Neurology 2006; 66:1485-9. [PMID: 16717206].

23. Zamvil SS, Slavin AJ. Does MOG Ig-positive AQP4-seronegative opticospinal inflammatory disease justify a diagnosis of NMO spectrum disorder? Neurol Neuroimmunol Neuroinflamm 2015; 2:e62-[PMID: 25635259].

24. Herges K, de Jong BA, Kolkowitz I, Dunn C, Mandelbaum G, Ko RM, Maini A, Han MH, Killestein J, Polman C, Goodyear AL, Dunn J, Steinman L, Axtell RC. Protective effect of an elastase inhibitor in a neuromyelitis optica-like disease driven by a peptide of myelin oligodendroglial glycoprotein. Mult Scler 2012; 18:398-408. [PMID: 22343184].

25. Matsushita T, Tateishi T, Isobe N, Yonekawa T, Yamasaki R, Matsuse D, Murai H, Kira J. Characteristic cerebrospinal fluid cytokine/chemokine profiles in neuromyelitis optica, relapsing remitting or primary progressive multiple sclerosis. PLoS One 2013; 8:e61835-[PMID: 23637915].

26. Smith E, Zarbock A, Stark MA, Burcin TL, Bruce AC, Foley P, Ley K. IL-23 is required for neutrophil homeostasis in normal and neutrophilic mice. J Immunol 2007; 179:8274-9. [PMID: 18056371].

27. Zhang Z, Zhong W, Spencer D, Chen H, Lu H, Kawaguchi T, Rosenbaum JT. Interleukin-17 causes neutrophil mediated inflammation in ovalbumin-induced uveitis in DO11.10 mice. Cytokine 2009; 46:79-91. [PMID: 19254849].

28. Liang SC, Long AJ, Bennett F, Whitters MJ, Karim R, Collins M, Goldman SJ, Dunussi-Joannopoulos K, Williams CM, Wright JF, Fouser LA. An IL-17F/A heterodimer protein is produced by mouse Th17 cells and induces airway neutrophil recruitment. J Immunol 2007; 179:7791-9. [PMID: 18025225].

29. Wu F, Cao W, Yang Y, Liu A. Extensive infiltration of neutrophils in the acute phase of experimental autoimmune encephalomyelitis in C57BL/6 mice. Histochem Cell Biol 2010; 133:313-22. [PMID: 20063008].

30. Barthelmes J, de Bazo AM, Pewzner-Jung Y, Schmitz K, Mayer CA, Foerch C, Eberle M, Tafferner N, Ferreiros N, Henke M, Geisslinger G, Futerman AH, Grosch S, Schiffmann S. Lack of ceramide synthase 2 suppresses the development of experimental autoimmune encephalomyelitis by impairing the migratory capacity of neutrophils. Brain Behav Immun 2015; 46:280-92. [PMID: 25697397].

31. Henke D, Rupp S, Gaschen V, Stoffel MH, Frey J, Vandevelde M, Oevermann A. Listeria monocytogenes spreads within the brain by actin-based intra-axonal migration. Infect Immun 2015; 83:2409-19. [PMID: 25824833].

Articles are provided courtesy of Emory University and the Zhongshan Ophthalmic Center, Sun Yat-sen University, P.R. China. The print version of this article was created on 11 April 2016. This reflects all typographical corrections and errata to the article through that date. Details of any changes may be found in the online version of the article.